Inorg. Chem. **2007**, *46*, 2503–2510

Self-Assembled Cationic Heterochiral Honeycomb-Layered Metal Complexes with the in Situ Generated Pyrimidine-2-carboxylato Bisdidentate Ligand. Hydrothermal Synthesis, Crystal Structures, Magnetic Properties, and Theoretical Study of $[M_2(\mu\text{-pymca})_3]OH\cdot H_2O$ ($M = Fe^{II}$, Co^{II})

Antonio Rodríguez-Diéguez,[†] Joan Cano,*[,‡] Raikko Kivekäs,[§] Abderrahmane Debdoubi,[||] and Enrique Colacio*[,†]

Departamento de Química Inorgánica, Facultad de Ciencias, Universidad de Granada, Av. Fuentenueva S/N, 18071 Granada, Spain, Departament de Química Inorgànica and Centre de Recerca en Química Teórica, Institució Catalana de Recerca i Estudis Avançats (ICREA), Universitat de Barcelona, Av. Diagonal 647, 08027 Barcelona, Spain, Department of Chemistry, Laboratory of Inorganic Chemistry, PO Box 55, FIN-00014 University of Helsinki, Finland, and Unité Calorimétrie et Matériaux, Université Abdelmalek Essaâdi, Faculté des Sciences, PO 212, Tétouan, Morroco

Received October 5, 2006

The hydrothermal reaction of 2-cyanopyrimidine and either $CoCl_2\cdot 6H_2O$ or $FeCl_2\cdot 4H_2O$ affords 2D isostructural coordination polymers $[M_2(\mu\text{-pymca})_3]OH\cdot H_2O$ (($M = Co^{II}$ (**1**) and Fe^{II} (**2**) pymca = pyrimidine-2-carboxylato). The bisdidentate ligand (pymca) that can be considered an intermediate between bipyrimidine and oxalato is generated in situ from the hydrolysis of 2-cyanopyrimidine. The structure of **1** and **2** consists of heterochiral (6,3) honeycomb layers, crystal water molecules, and OH^- anions, the latter playing a template and balancing charge role in the structure. Both compounds exhibit antiferromagnetic interactions between metal ions through the pyrimidine-2-carboxylate bridging ligand. Compound **1** is a spin-canted antiferromagnet leading to weak ferromagnetism at $T_c < 10$ K with a coercitive field of 580 Oe, whereas compound **2** is an antiferromagnet with $T_N = 21$ K. Fit of the variable-temperature magnetic susceptibility data of **2** to the empirical equation for a regular honeycomb with $S = 1$ derived from Monte Carlo simulations leads to the following parameters: $J = -4.57(2)$ cm^{-1} and $g = 2.300(4)$. Density functional calculations have been used to explain the magnetic coupling in **2**.

Introduction

Multidimensional coordination polymers have attracted much attention in recent years not only because of their structural and topological novelty but also because of their potential applications as molecule-based functional materials in fields such as electrical conductivity, molecular magnetism, molecular absorption, catalysis, optical materials, etc.[1] Molecule-based magnetic materials have been commonly prepared through a bottom-up approach, connecting paramagnetic transition metal ions with appropriate bridging ligands. The metal ions are the source of magnetic moments, whereas the bridging ligands allow for the magnetic exchange coupling between the magnetic centers.[1e] Consequently, the sign and magnitude of the magnetic exchange interaction primarily depend on the nature of the bridging ligand and interacting metal ions.[2] It should be pointed out that only a

* To whom correspondence should be addressed. E-mail: ecolacio@ugr.es. (E.C.), joancano@antares.qu.ub.es (J.C.)
[†] Universidad de Granada.
[‡] Institució Catalana de Recerca i Estudis Avançats.
[§] University of Helsinki.
[||] Université Abdelmalek Essaâdi.

(1) (a) Moulton B.; Zaworotko, M. J. *Chem. Rev.* **2001**, *34*, 319. (b) Oxtoby, A.; Champness, N. R. *Coord. Chem. Rev.* **2003**, *246*, 145. (c) Janiak, C. *Dalton Trans.* **2003**, 2781. (d) Kitagawa, S.; Kitaura, R.; Noro, S.-I. *Angew. Chem., Int. Ed.* **2004**, *43*, 2334. (e) *Magnetism: Molecules to Materials*, Miller, J. S.; Drillon, M., Eds.; Wiley-VCH: Weinheim, Germany, 2001. (f) García, Y.; Niel, V.; Muñoz M. C.; Real, J. A. *Top. Curr. Chem.* **2004**, *233*, 229 and references therein. (g) Batten S. R.; Murray, K. S. *Coord. Chem. Rev.*, **2003**, 246, 103 and references therein.
(2) Kahn, O. *Molecular Magnetism*; VCH: Weinheim, Germany, 2001.

10.1021/ic061908e CCC: $37.00
Published on Web 02/28/2007

Chart 1

2,2′-bipyrimidine (N4 donor set, no charge) | pyrimidine-2-carboxylato (N2O2 donor set, charge -1) | oxalato (O4 donor set, charge -2)

few polyatomic bridging ligands (cyanide, oxalate, dicyanamide, azide, bipyrimidine, imidazol, carboxylate, etc.) have been shown to be able to mediate strong magnetic coupling between transition metal ions that, in some cases, leads to bulk magnetic ordering.[1e] Therefore, there is still great interest in the search for new bridging ligands, which can produce new magnetic materials with intriguing structures and magnetic properties. Both 2,2′-bipyrimidine (bpym) and oxalate (ox) bisdidentate bridging ligands have been extensively used in the construction of a great variety of multidimensional polynuclear complexes that exhibit interesting structures and magnetic properties.[3,4] Bpym generates, among other systems, neutral honeycomb-layered networks with alternating bridging ligands (ox/bpym and azide/bpym) and magnetic interactions,[5] whereas ox gives rise to tris(oxalate)metalate-based honeycomb 2D and 3-connected decagon bimetallic anionic networks of general formula $[M^{II}M^{III}(ox)_3]^-$ which magnetically order at temperatures as high as 48 K.[4,6] The right choice of the template cation in these latter systems allows for the introduction of new physical properties in addition to the long-range magnetic ordering arising from the anionic network, thus obtaining polyfunctional magnetic materials.[4c] Ligands offering donor atoms set and charge-balance requirements other than those of bpym and ox may afford advantages in the design of new functional magnetic materials. In this context, we report here the structural and magnetic properties of two coordination polymers $[M_2(\mu\text{-pymca})_3]OH\cdot H_2O$ (M = Co^{II} (**1**) and Fe^{II} (**2**)) containing a new bisdidentate bridging ligand, pyrimidine-2-carboxylate (pymca), that can be considered as one-half bpym and one-half ox and consequently exhibits a N_2O_2 donor set and a charge of −1, which is intermediate between those of bpym and ox (Chart 1). It should be noted that the crystal structure of the pymca-containing mononuclear complex, $[Co(pymca)(en)_2](CF_3O_3S)_2\cdot 2H_2O$, has been previously reported.[7] In this case, however, the pymca ligand (an impurity of the commercial bpym) exhibits a nonbridging N,O-bidentate coordination mode.

Experimental Section

All analytical reagents were purchased from commercial sources and used without further purification. 2-Cyanopyrimidine was prepared according to a previously described procedure.[8]

Synthesis. Orange crystals of $[Co_2(\mu\text{-pymca})_3]OH\cdot H_2O$ (**1**) were obtained in a yield of 72% by heating a mixture of $CoCl_2\cdot 6H_2O$ (0.113 g, 0.47 mmol), 2-cyanopyrimidine (0.050 g, 0.47 mmol), and H_2O (10 mL) in a 23 mL Teflon-lined acid digestion bomb at 190 °C for 12 h under autogenous pressure followed by slow cooling to room temperature. Anal. Calcd for $C_{15}H_{12}N_6O_8Co_2$: C, 34.47; H, 2.30; N, 16.09. Found: C, 34.29; H, 1.97; N, 16.35. IR (KBr, cm^{-1}): 3451, ν(OH); 3088, ν(CH); 1629, δ(OH); 1589, $\nu(COO)_{as}$; 1384, $\nu(COO)_s$.

Red crystals of **2** were obtained in a yield of 82% by heating a mixture of $FeCl_2\cdot 4H_2O$ (0.120 g, 0.60mmol), 2-cyanopyrimidine (0.063 g, 0.60 mmol), and H_2O (8 mL) in a 23 mL Teflon-lined acid digestion bomb at 180 °C for 12 h under autogenous pressure followed by slow cooling to room temperature. Anal. Calcd for $C_{15}H_{12}N_6O_8Fe_2$: C, 34.88; H, 2.32; N, 16.28. Found: C, 35.18; H, 2.02; N, 16.48. (KBr, cm^{-1}): 3452, ν(OH); 3088, ν(CH); 1627, δ(OH); 1586, $\nu(COO)_{as}$; 1383, $\nu(COO)_s$.

Physical Measurements. Elemental analyses were carried out at the Instrumentation Scientific Centre of the University of Granada on a Fisons-Carlo Erba analyzer model EA 1108. The IR spectra on powdered samples were recorded with a ThermoNicolet IR200FTIR by using KBr pellets. Magnetization and variable-temperature (1.9−300 K) magnetic susceptibility measurements on polycrystalline samples were carried out with a Quantum Design SQUID device operating at different magnetic fields. Magnetization versus applied field measurements were carried out at 2.0 K in the field range of 0−5 T. Alternating current susceptibility measurements were performed in the frequency range of 10−100 Hz and under an oscillating magnetic field of 1 Oe. The experimental susceptibilities were corrected for the diamagnetism of the constituent atoms by the use of Pascal's tables.

X-ray Crystallography. Single-crystal data collections for **1** and **2** were carried out at on a Bruker Smart Apex diffractometer using

(3) (a) De Munno, G.; Julve, M. In *Metal−Ligand Interactions. Structure and Reactivity*; Russo, N., Salahub, D. R., Eds.; Kluwer: Dordrecht, The Netherlands, 1996; p 139 and references therein. (b) De Munno, G.; Lloret, F.; Julve, M. In *Magnetism: A Supramolecular Function*; Kahn, O., Ed.; Kluwer: Dordrecht, The Netherlands, 1996; p 555 and references therein. (c) Triki, S.; Thétiot, F.; Vandevelde, F.; Sala-Pala, J.;. Gómez-García, C. J. *Inorg. Chem.* **2005**, 44, 4086 and references therein.

(4) Some reviews: (a) Decurtins, S.; Pellaux, R.; Hauser, A.; Von Arx, M. E. In *Magnetism: A Supramolecular Function*; Kahn, O, Ed.; Kluwer: Dordrecht, The Netherlands, 1996; p 487 and references therein. (b) Pilkington, M.; Decurtins S. In *Comprehensive Coordination Chemistry II. From Biology to Nanaotechnology*; MacCleverty, J. A., Meyer, T. J., Eds.; Elsevier: Amsterdam, 2004; Vol 7, p 177. (c) Pilkington, M.; Decurtins S. *Crystal Design: Structure and Function*; Desiraju, G. R., Ed.; Perspectives in Supramolecular Chemistry; Wiley: West Sussex, U.K., 2003; Vol 7, pp 275−323. (d) Clément, R.; Decurtins, S.; Gruselle, M.; Train, C. *Monastsh. Chem.* **2003**, *134*, 117 and references therein.

(5) (a) De Munno, G.; Armentano, D.; Julve, M.; Lloret, F.; Lescouëzec, R.; Faus, J. *Inorg. Chem.* **1999**, *38*, 2234. (b) Armentano, D.; De Munno, G; Lloret, F.; Julve, M.; Curély, J.; Babb, A. M.; Lu, J. Y. *New J. Chem.* **2003**, *27*, 161. (c) De Munno, G.; Julve, M.; Viau, G.; Lloret, F.; Faus, J.; Viterbo, D. *Angew. Chem., Int. Ed.* **1996**, *35*, 1807. (d) De Munno, G.; Poerio, T.; Viau, G.; Julve, M.; Lloret, F.; Journaux, Y.; Riviere, E. *Chem. Commun.* **1996**, *22*, 2587.

(6) (a) Tamaki, H.; Zhong, Z. J.; Matsumoto, N.; Kida, S.; Koikawa, M.; Achiwa, N.; Hashimoto, I.; Okawa, H. *J. Am. Chem. Soc.* **1992**, *114*, 6974. (b) Day, P. *J. Chem. Soc., Dalton Trans.* **1997**, 701. (c) Coronado, E.; Galán-Mascarós, J. R.; Martí-Gastaldo, C. *Inorg. Chem.* **2006**, *45*, 1882.

(7) Antolic, S.; Kojic-Prodic, B.; Lovric, J. *Acta Crystallogr.* **2000**, *C56*, e51.

(8) Case, F. H.; Koft, E. *J. Am. Chem. Soc.* **1959**, *81*, 905.

Table 1. Crystallographic Data and Structural Refinement Details for Compounds

	1	**2**
empirical formula	$C_{15}H_{12}Co_2N_6O_8$	$C_{15}H_{12}Fe_2N_6O_8$
fw	522.17	516.01
cryst syst	trigonal	trigonal
space group	$P3_1m$	$P3_1m$
a (Å)	9.548(5)	9.6956(8)
c (Å)	6.077(5)	6.0530(10)
V (Å^3)	479.8(5)	492.78(10)
Z	1	1
T (C)	−120	−173
λ (Å)	0.71073	0.71073
ρ (g cm^{-3})	1.807	1.739
μ (cm^{-1})	17.88	15.30
GOF	1.144	1.194
R1[a] [$I > 2\sigma(I)$]	0.0704	0.0744
wR2[b] [$I > 2\sigma(I)$]	0.1878	0.2052
Flack's parameter x	0.20(10)	0.24(7)

[a] $R1 = \Sigma||F_o| - |F_c||/\Sigma|F_o|$. [b] $wR2 = \{\Sigma[w(F_o^2 - F_c^2)^2]/\Sigma[w(F_o^2)^2]\}^{1/2}$.

Table 2. Selected Interatomic Distances (Å) and Angles (deg)[a]

	1	**2**
M−O1	2.079(2)	2.0940(16)
M−N	2.113(3)	2.163(2)
O1−C4	1.349(4)	1.315(3)
N−C1	1.190(3)	1.196(2)
N−C2	1.511(6)	1.551(5)
C1−C4	1.575(6)	1.581(5)
C2−C3	1.444(7)	1.415(5)
O1−M−O1[b]	93.39(10)	94.42(7)
O1−M−N	79.08(10)	77.11(7)
O1−M−N[c]	169.76(11)	167.97(8)
N−M−N[c]	94.39(11)	94.40(7)

[a] M equals Co^{II} for **1** and Fe^{II} for **2**. [b] Symmetry transformations used to generate equivalent atoms: $-y + 1, x - y, z$. [c] Symmetry transformations used to generate equivalent atoms: $-x + y + 1, -x + 1, z$.

graphite-monochromatized Mo Kα radiation. A total of 2586 and 3060 reflections, giving 579 ($R_{int} = 0.0581$) and 755 unique ($R_{int} = 0.0268$) reflections, were collected for **1** and **2**, respectively. The structures are isostructural, and they were solved by direct methods and refined on F^2 by the SHELXL97 program.[9] Oxygen atoms O2 and O3 occupy symmetry element 3*m*. The O2 atom was assumed to belong to the OH^- ion because of the H bond contact distance to C3, and the O3 atom was assumed to belong to the water molecule. For both compounds, all non-hydrogen atoms were refined with anisotropic displacement parameters. Hydrogen atoms bonded to O2 and O3 could not be reliably positioned, but the rest of the hydrogen atoms were treated as riding atoms using the SHELX97 default parameters. A summary of the crystallographic data and structure refinements is given in Table 1, whereas selected bond lengths and angles are gathered in Table 2.

Computational Details. Calculations have been carried out with the hybrid B3LYP method,[10−12] as implemented in the Gaussian 03 program.[13] Double- and triple-ζ-quality basis sets proposed by Ahlrichs and co-workers have been used for nonmetal and metal atoms, respectively.[14,15] The broken-symmetry approach has been employed to describe the unrestricted solutions of the antiferromagnetic spin states.[16−22] The atomic spin densities have been obtained from a natural bond orbital analysis.[23−25] We have built a model where the peripheral ligands are ammonia groups (Figure 7). All metal−ligand distances have been optimized in order to describe properly the ligand that affects the metal ion.

Monte Carlo Simulations. To simulate the magnetic behavior of compound **2**, we have used the Monte Carlo method (MC), and the spin moments have been considered as classical vectors (classical spin approach). MC methods allow us to study large systems, and the classical spin approach calculates the energy of the different configurations in a simple way. With MC methods, from the spin flip probabilities and with the use of a metropolis algorithm, we can generate a sampling where the more present states are those with a more important contribution in the partition function. This sampling allows us to calculate the average magnetization at a given temperature. The molar magnetic susceptibility can be obtained from the fluctuations in the magnetization through eq 1, where $\langle M \rangle$ and $\langle M^2 \rangle$ are the mean values of the magnetization and its square, respectively, and N, β, and k have their usual meanings.

$$\chi_M T = N\beta^2/k(\langle M^2 \rangle - \langle M \rangle^2) \quad (1)$$

In all simulations, the number of MC steps for each temperature is $5 \times 10^6/T$ (T in K). Thus, we have included more steps in the sampling at low temperatures where the correct equilibrium requires more recorded data. Ten percent of the MC steps are employed for the thermalization of the system; thus we have stocked the physical properties when the equilibrium is reached. A model of 20 × 20

(9) Sheldrick, G. M. *SHELX97*; University of Göttingen: Göttingen, Germany, 1997.
(10) Becke, A. D. *Phys. Rev. A* **1988**, *38*, 3098.
(11) Lee, C. T.; Yang, W. T.; Parr, R. G. *Phys. Rev. B* **1988**, *37*, 785.
(12) Becke, A. D. *J. Chem. Phys.* **1993**, *98*, 5648.
(13) Frisch, M. J.; Trucks, G. W.; Schlegel, H. B.; Scuseria, G. E.; Robb, M. A.; Cheeseman, J. R.; Montgomery, J.; Vreven, T.; Kudin, K. N.; Burant, J. C.; Millam, J. M.; Iyengar, S. S.; Tomasi, J.; Barone, V.; Mennucci, B.; Cossi, M.; Scalmani, G.; Rega, N.; Petersson, G. A.; Nakatsuji, H.; Hada, M.; Ehara, M.; Toyota, K.; Fukuda, R.; Hasegawa, J.; Ishida, M.; Nakajima, T.; Honda, Y.; Kitao, O.; Nakai, H.; Klene, M.; Li, X.; Knox, J. E.; Hratchian, H. P.; Cross, J. B.; Bakken, V.; Adamo, C.; Jaramillo, J.; Gomperts, R.; Stratmann, R. E.; Yazyev, O.; Austin, A. J.; Cammi, R.; Pomelli, C.; Ochterski, J. W.; Ayala, P. Y.; Morokuma, K.; Voth, G. A.; Salvador, P.; Dannenberg, J. J.; Zakrzewski, V. G.; Dapprich, S.; Daniels, A. D.; Strain, M. C.; Farkas, O.; Malick, D. K.; Rabuck, A. D.; Raghavachari, K.; Foresman, J. B.; Ortiz, J. V.; Cui, Q.; Baboul, A. G.; Clifford, S.; Cioslowski, J.; Stefanov, B. B.; Liu, G.; Liashenko, A.; Piskorz, P.; Komaromi, I.; Martin, R. L.; Fox, D. J.; Keith, T.; Al-Laham, M. A.; Peng, C. Y.; Nanayakkara, A.; Challacombe, M.; Gill, P. M. W.; Johnson, B.; Chen, W.; Wong, M. W.; Gonzalez, C.; Pople, J. A. *Gaussian 03*, Revision C.02; Gaussian, Inc.: Wallingford, CT, 2004.
(14) Schäfer, A.; Horn, H.; Ahlrichs, R. *J. Chem. Phys.* **1992**, *97*, 2571.
(15) Schäfer, A.; Huber, C.; Ahlrichs, R. *J. Chem. Phys.* **1994**, *100*, 5829.
(16) Ruiz, E.; Alemany, P.; Alvarez, S.; Cano, J. *Inorg. Chem.* **1997**, *36*, 3683.
(17) Ruiz, E.; Alemany, P.; Alvarez, S.; Cano, J. *J. Am. Chem. Soc.* **1997**, *119*, 1297.
(18) Ruiz, E.; Alvarez, S.; Rodríguez-Fortea, A.; Alemany, P.; Puoillon, Y.; Massobrio, C. In *Magnetism: Molecules to Materials*; Miller, J. S., Drillon, M., Eds.; Wiley-VCH: Weinheim, Germany, 2001; Vol 2, p 5572.
(19) Ruiz, E.; Cano, J.; Alvarez, S. *Chem.—Eur. J.* **2005**, *11*, 4767.
(20) Ruiz, E.; Rodriguez-Fortea, A.; Alvarez, S.; Verdaguer, M. *Chem.—Eur. J.* **2005**, *11*, 2135.
(21) Ruiz, E.; Rodriguez-Fortea, A.; Cano, J.; Alvarez, S. *J. Phys. Chem. Solids* **2004**, *65*, 799.
(22) Ruiz, E.; Rodriguez-Fortea, A.; Cano, J.; Alvarez, S.; Alemany, P. *J. Comput. Chem.* **2003**, *24*, 982.
(23) Weinhold, F.; Carpenter, J. E. *J. Mol. Struct.* **1988**, *42*, 189.
(24) (a) Weinhold, F.; Landis, C. R. *Valency and Bonding: A Natural Bond Orbital Donor-Aceptor Perspective*; Cambridge University Press, Cambridge, U.K., 2005. (b) Weinhold, F.; Carpenter, J. E. *The Structure of Small Molecules and Ions*: Plenum: New York, 1988.
(25) Reed, A. E.; Curtiss, L. A.; Weinhold, F. *Chem. Rev.* **1988**, *88*, 899.
(26) Cano, J.; Journaux, J. In *Magnetism: Molecules to Materials*; Miller, J. S., Drillon, M., Eds.; Wiley-VCH, Weinheim, Germany, 2005; Vol 5.

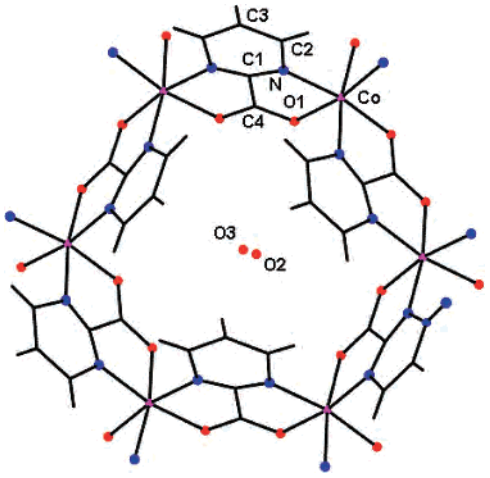

Figure 1. View of the hexagonal ring motif of the complexes.

sites has been used, and periodic boundary conditions have been introduced in all simulations. Deeper details on MC simulations can be found in ref 26.

Results and Discussion

Synthesis. It has long been known that nitriles can be hydrolyzed to carboxylic acids and ammonia. In neutral solution the rate of this reaction is very slow. However, the use of basic or acid conditions and high temperatures dramatically increases the rate of the reaction.[27] Metal ions are powerful activators of nitriles toward nucleophilic attack by OH^-/H_2O. This activation results in an enhancement of the rate of hydrolysis, leading to amides and/or amide complexes. Indeed, hydration processes which give carboxylic acids are rare.[27] Stabilization of the carboxamide upon complexation is the first factor explaining the selectivity of the hydrolysis provided by metal ions. However, hydrothermal conditions (high pressure and temperature) must favor the complete hydrolysis of nitriles and consequent formation of metal−carboxylate complexes.[28] Because the reaction of 2-cyanopyrimidine with metal(II) chlorides in water using mild conditions (atmospheric pressure and room temperature) leads to bis(carboxamide)metal(II) mononuclear complexes,[29] we decided to use hydrothermal conditions in an attempt to obtain polynuclear pyrimidine-2-carboxylate-bridged complexes. As expected, during the course of the hydrothermal reaction, the pymca ligand was generated in situ, leading to compounds **1** and **2**.

Crystal Structures. The crystal structures were determined by single-crystal X-ray crystallography and found to be isostructural. The structures are made of cationic layers $[M_2(pymca)_3]_n^{n+}$ ($M = Co^{II}$ and Fe^{II}), crystal water molecules, and OH^- anions, which play a template and balancing charge role in the structure. Each metal exhibits a distorted octahedral MN_3O_3 coordination environment with C_3 symmetry, which is formed by the coordination of three N,O-bidentate pymca ligands in fac disposition (Figure 1). M−O distances for **1** and **2** are 2.079(2) and 2.0940(16) Å, respectively, and are similar to those found for oxalate-bridged complexes, whereas M−N distances are 2.113(3) and 2.163(2) Å, respectively, and are close to those found for bipyrimidine-bridged complexes.[5b,30] The O−M−N bite angles are 79.08(10)° for **1** and 77.11(7)° for **2,** but the rest of the cis O−M−N, O−M−O, and N−M−N angles are larger than 90°, being 93.39(10)−94.39(11)° for **1** and 94.42(7)−94.90(7)° for **2**. The distortion of the MN_3O_3 octahedron is mainly due to the small bite angle of the pymca ligand. Because of this, trans O−M−N angles of 169.76(11)° for **1** and 167.97(8)° for **2** deviate significantly from linearity. Tris(bidentate) MN_3O_3 units display a propeller-like chirality and can therefore exist as MΔ and MΛ enantiomeric forms. Each chiral unit is linked to other three neighboring ones to produce (6,3) honeycomb 2D cationic layers in the *ab* plane (Figure 2). Because each metal ion is related to the neighboring ones by mirror planes going through the atoms C1, C3, and C4 of the pymca ligand, each pair of neighboring metal ions has opposite chirality. This heterochiral cationic network is topologically analogous to that observed for anionic 2D oxalate-bridged bimetallic complexes. If the 2D cationic network $[M_2(pymca)_3]_n^{n+}$ were homochiral, a 3D architecture similar to that observed for homochiral oxalate-bridged bimetallic complexes would be expected.[4] Within the honeycomb layers, M···M distances across the pymca ligands and through the longest diagonal of the hexagonal ring are 5.513(3) and 11.025(6) Å for **1** and 5.5978(5) and 11.1955(9) Å for **2.** It should be noted that, on one side of the layer and within each hexagonal ring, the pyrimidine rings of the ligands are alternatively tilted (32.6(2)° for **1** and 33.11(5)° for **2**) toward and away from the normal to the ring. Consequently, on the other side of the layer, carboxylate groups follow the opposite sequence (Figure 1). The dihedral angle between the planes of neighboring ligands is 86.6(2)° for **1** and 87.05(5)° for **2**.

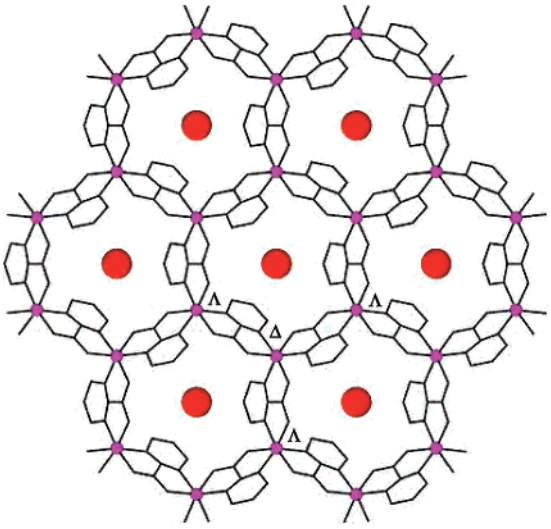

Figure 2. View along *c*-axis of the 2D network of the complexes. OH^- anions are highlighted.

(27) Kukushkin, V. Y.; Pombeiro, A. J. L. *Inorg. Chim. Acta* **2005**, *358*, 1.
(28) Martin, J. D.; Hess, R. F.; Boyle, P. D. *Inorg. Chem.* **2004**, *43*, 3242.
(29) Colacio, E.; Debdoubi, A.; Rodríguez-Diéguez, A. Unpublished results.
(30) De Munno, G.; Julve, M.; Lloret, F.; Faus, J.; Caneschi, A. *J. Chem. Soc., Dalton Trans.* **1994**, 1175.

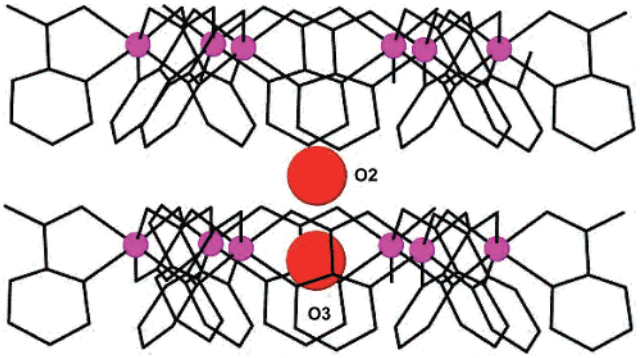

Figure 3. Perspective view of the location of the OH^- anions (O2) and water molecules (O3) between the sheets.

In both cases, the O2 oxygen atoms of the OH^- anions lie on the normal through the barycenters of the hexagonal rings and are therefore equidistant from the three C3 atoms that are closer to the normal and are also equidistant from the oxygen atoms of the three carboxylate groups that are closer to the normal in the neighboring layer (Figure 3). The C3···O2 and O2···O3 separations of 2.954(9) and 2.576(16) Å in **1** and 2.910(6) and 2.573(15) Å in **2** indicate hydrogen bonds between the atoms. In both structures, each OH^- anion and crystal water molecule can be considered as encapsulated by the set of six alternating in orientation pymca ligands defining the hexagonal ring.

The shortest M···M interlayer separations along the *c*-axis are 6.077(5) Å and 6.0530(10) Å for **1** and **2**, respectively.

To the best of our knowledge, the structure of these compounds is unique because (i) they represent the first examples of 2D coordination polymers containing cationic heterochiral honeycomb networks with bisdidentate ligands and (ii) the honeycomb network is made of only one type of metal and only one type of bisdidentate ligand. In this regard, it should be mentioned that oxalato-bridged honeycomb layers, $[M^{II}M^{III}(ox)_3]^-$, are made of two types of metal ions. Moreover, although neutral honeycomb networks with only one type of metal ion have been reported, they contain two different kinds of bridging ligands (bpym/ox,[5b] bpym/azide,[5d] end-on/end-to-end azide[31]).

Magnetic Properties. The temperature-dependence of the $\chi_M T$ product (χ_M is the molar susceptibility per Co atom) for **1** at different applied magnetic fields is given in Figure 4. The value of $\chi_M T$ at room temperature of 2.83 $cm^3\ mol^{-1}$ K substantially exceeds the spin-only value of 1.875 $cm^3\ mol^{-1}$ K expected for an uncoupled high-spin Co^{II} ($S = {}^3/_2$) ion with $g = 2$, thus indicating that an important orbital contribution due to the distorted octahedral Co^{II} ion exists. In a magnetic field of 0.5 T, the $\chi_M T$ product continuously decreases with the temperature, reaching a value of 0.1 $cm^3\ mol^{-1}$ K at 2 K. This behavior is a consequence of both the spin−orbit coupling effects and weak antiferromagnetic interactions. The antiferromagnetic nature of the interaction is clearly supported by the incipient maximum that is observed around 10 K in the magnetic susceptibility plot (inset Figure 4). In a field of 0.03 T, however, the $\chi_M T$ values

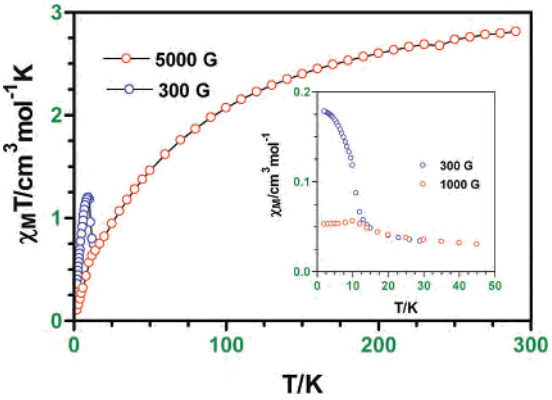

Figure 4. Temperature-dependence of the $\chi_M T$ product for **1** at different magnetic fields (the solid line is just an eye-guide). The inset represents the thermal variation of the susceptibility at different magnetic fields.

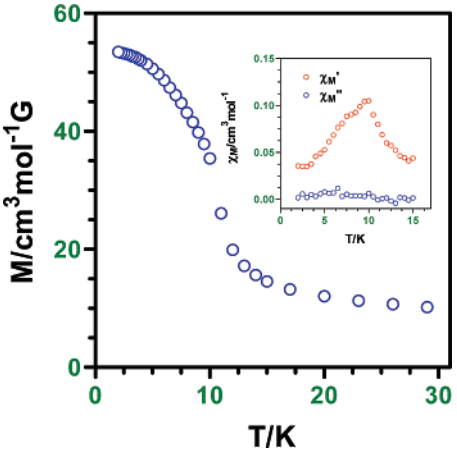

Figure 5. Field-cooled magnetization of **1** under an external field of 20 Oe. The inset shows the temperature-dependence of the in-phase and out-of-phase *ac* magnetic susceptibilities.

rise sharply at around 12 K, reach a maximum of 1.25 $cm^3\ mol^{-1}$ K at 10 K, and then decrease rapidly toward 0.30 $cm^3\ mol^{-1}$ K at 2 K. This low-temperature behavior suggests a ferromagnetic phase transition. The field-cooled magnetization at 0.03 T confirms the occurrence of a magnetic ordering below 10 K (Figure 5). The isothermal magnetization at 2 K shows linear dependence with field, attaining a value of 1240 $cm^3\ G\ mol^{-1}$ at 5 T, which is significantly smaller than the theoretical saturation magnetization value (M_s) of 16755 $cm^3\ G\ mol^{-1}$ with $g = 2$. The magnetic hysteresis loop for **1** shows values of coercitive field and remnant magnetization (M_r) of 580 G and 94 $cm^3\ G\ mol^{-1}$, respectively, which are typical of a soft magnet. All the above magnetic properties are characteristics of a canted antiferromagnet, leading to weak ferromagnetism at low temperature. The canting angle is related to M_r and M_s through $\sin(\alpha) = M_r/M_s$ and is estimated to be 0.32°. In **1** the in-phase signal (χ_M') appears at 10 K and is frequency-independent whereas the out-of-phase signal (χ_M'') is not observed (inset Figure 5). The same *ac* susceptibility behavior has been observed for other 2D and 3D polynuclear Co^{II} complexes.[32] In all these systems the magnetic moment from canting is so small that the loss of energy related to the out-of-phase signal is negligible. The spin-canting in **1** must be a consequence of both the local anisotropy of the high-spin Co^{II} ions and the antisymmetric

(31) Escuer, A.; Cano, J.; Goher, M. A. S.; Journaux, Y.; Lloret, F.; Mautner, F. A.; Vicente, R. *Inorg. Chem.* **2000**, *39*, 4688.

Table 3. Energy Gaps (Δ, in cm^{-1}) between the Symmetrical and Antisymmetrical SOMOs; Atomic Spin Density (ρ, in Electrons) on the Iron Atom; Energy (E, in hartrees) of the First Ligand Orbital Involved in the Building of SOMOs; and Calculated and Experimental Exchange Coupling Constants (J, in cm^{-1}) for Models **ox**, **pymca**, and **bpm**

model	E (ϕ_1)[a]	Δ ($x^2 - y^2$)	Δ (z^2)	Δ (yz)	Δ (xy)	r	J_{calc}	J_{exp}	ref
ox	0.196	2471	610	805	134	3.75	−7.4	−6.6/ −8.0	33
pymca	−0.052[b]	2236	810	770	88	3.78	−2.9	−4.6	this work
bpm	−0.223	1743	546	562	204	3.79	−1.5	−3.1/ −4.1	5b, 34

[a] See Figure 8. [b]In this case this orbital is split in two, as one part is localized on the oxygen atoms of the ligand and the other on the nitrogen atoms; therefore, an average value is given.

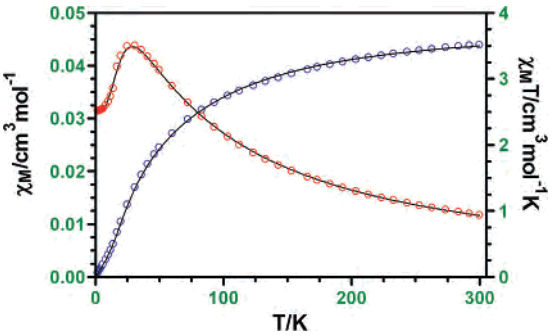

Figure 6. Temperature-dependence of the χ_M and $\chi_M T$ product for **2**. The solid line is the best-fit curve to the theoretical eq 2.

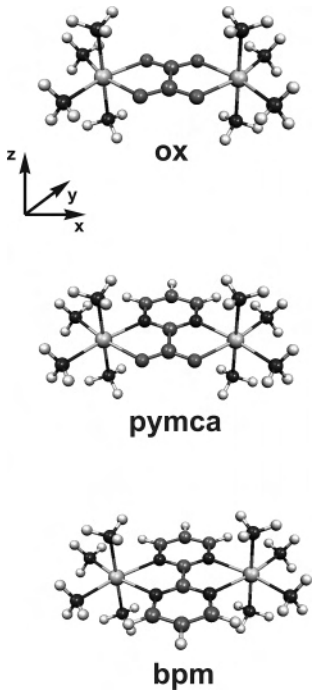

Figure 7. Perspectives of models **ox**, **pymca**, and **bpm** and considered axis orientation.

exchange interaction, which is compatible with the acentric character of the space group of **1** and with the fact that the C_3 axis is perpendicular to the cobalt-containing plane.[33] The 3D long-range order in **1** is only possible through weak interlayer interactions, and this is the reason why T_c is relatively low.

In a magnetic field of 0.5 T, the interlayer exchange interaction is overcome, and consequently, the $\chi_M T$ vs T plot does not show the abrupt increase at around 12 K. Nevertheless, because the antiferromagnetic intralayer interaction is still present, a maximum is observed in the χ_M vs T curve.

The temperature-dependence of χ_M and $\chi_M T$ for **2** (χ_M is the molar magnetic susceptibility per Fe(II) ion) in an applied field of 0.5 T is displayed in Figure 6. At room temperature, the $\chi_M T$ product (3.51 $cm^3\ mol^{-1}\ K$) is slightly higher than the spin-only value expected for high-spin Fe(II) ions of 3 $cm^3\ mol^{-1}\ K$ with $S = 2$ and $g = 2$, which is probably due to the existence of a small orbital contribution from the distorted octahedral Fe(II) ion. The $\chi_M T$ product shows a continuous decrease with decreasing temperature to reach a value of 0.063 $cm^3\ mol^{-1}\ K$ at 2 K. This behavior suggests the presence of an antiferromagnetic interaction between Fe(II) ions through the pymca bridging ligand. In keeping with this, the thermal variation of χ_M shows a maximum of 0.045 $cm^3\ mol^{-1}$ near 24 K. Below this temperature, we were able to state that the the χ_M value approaches a value of 0.030 $cm^3\ mol^{-1}$ by extrapolating the temperature to zero. This value accounts for about two-thirds of the value of the maximum, which is typical of an antiferromagnet. The $d(\chi_M T)/dT$ versus T curve shows a maximum value at 21 K for the Néel temperature. Therefore, the antiferromagnetic coupling between Fe(II) ions gives rise to an antiferromagnetic ordering below 21 K. At low temperature χ_M is independent of the applied magnetic field, thus indicating that compound **2** does not behave as a spin-canted antiferromagnet. The different magnetic behavior for **1** (spin-canted antiferromagnet) and **2** (antiferromagnet) may be a consequence of the higher anisotropy of the octahedral Co(II) ion compared with that of the octahedral Fe(II) ion.

To facilitate the study of the magnetic properties, we have used Monte Carlo simulations only to find an empirical law able to reproduce the magnetic behavior of a regular honeycomb constituted from S_i local spin moments. For this case, using the next phenomenological Heisenberg Hamiltonian

$$H = -J[\sum_{i=1}^{\infty}\sum_{j=1}^{\infty}\hat{S}_{i,j}\cdot\hat{S}_{i,j+1} + \sum_{i=0}^{\infty}(\sum_{j=0}^{\infty}\hat{S}_{2i+1,2j+1}\cdot\hat{S}_{2i+2,2j+1} + \sum_{j=0}^{\infty}\hat{S}_{2i+2,2j+2}\cdot\hat{S}_{2i+3,2j+2})]$$

the empirical law takes the next form

(32) Tian, Y.-Q.; Cai, C.-X.; Ren, X.-M.; Duan, C.-Y.; Xu, Y.; Gao, S.; You, X.-Z. *Chem.—Eur. J.* **2003**, *9*, 5673.
(33) (a) Dzyaloshinski, I. *J. Phys. Solids* **1958**, *4*, 241. (b) Moriya T.; *Phys. Rev.* **1960**, *120*, 91.

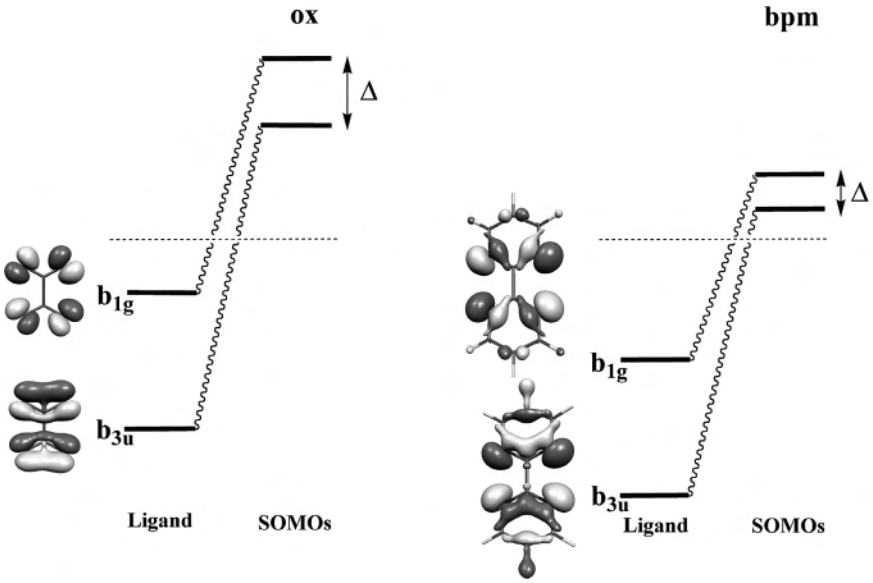

Figure 8. Qualitative diagram of the building of SOMOs from the ligand orbitals in models **ox**, **pymca**, and **bpm**. Δ represents the energy gap between the SOMOs. The location of the metal d orbital is pointed out with a dashed line.

$$\chi = \frac{g^2}{8|J|}\frac{0.4958 - 0.87293\beta + 2.3033\beta^2 + 0.96542\beta^3}{1.5546 - 2.1086\beta + 3.7612\beta^2 + 2.7411\beta^3 + \beta^4} \quad (2)$$

where $\beta = T/[|J|S(S+1)]$, T being the temperature, S the local spin moment, J the exchange coupling constant, and g the g factor. The susceptibility data for **2** have been fitted to eq 2. A very satisfactory fit has been obtained with the following parameters: $J = -4.57(2)$ cm^{-1}, $g = 2.300(4)$, and $R = 4.2 \times 10^{-6}$. This is an intermediate J value between those observed for oxalate[34] and bipyrimidine-bridged Fe(II) complexes,[5b,35] which are in the ranges of -6.6 to -8.8 cm^{-1} and -3.4 to -4.1 cm^{-1}, respectively.

To explain the exchange magnetic coupling observed for **2**, we have carried out electronic structure calculations based on the density functional theory (DF). We have compared the magnetic exchange coupling constants with those observed for similar complexes with bipyrimidine (bpm) or oxalate (ox) bridging ligands (Table 3). In fact, ligand pymca can be seen as an intermediate case between bpm and ox ligands. Dinuclear complex models have been named with the corresponding bridging ligand label (see Figure 7). They present a similar electronic configuration where the *xz* orbital is the only nonmagnetic orbital. We have evaluated the exchange coupling constants on the three models. Results are displayed in Table 3 and are in quantitative agreement with the experimental data found in the literature. Thus, the strongest magnetic coupling is that mediated by the oxalate ligand, whereas the weakest magnetic interaction is that observed in model **bpm** where the bipyrimidine ligand connects the iron(II) ions. For model **pymca**, such as that observed for **2**, an intermediate J value is found. Figure 8 shows some ligand orbitals involved in the formation of the single-occupied molecular orbitals (SOMOs) in the high-spin state that is obtained by a parallel layout of the spin moments of the two metal ions. DF calculations on the free ligands show that their energies depend on the ligand, following the next order of **bpm** < **pymca** < **ox** (Table 3 and Figure 8). Thus, despite the fact that the nitrogen donor atom is less electronegative than the oxygen atom, the oxalate has the least stable orbitals; consequently, the bpm orbitals are closer to the metal d orbitals. This can be due to the fact that the σ electronic density is more delocalized in the bipyrimidine ligand, thus decreasing the antibonding interactions on the common skeleton (see molecular orbitals in Figure 8). Also, in these orbitals, some bonding interactions that appear in the ring of bpm ligand cannot be present in the ox ligand. Following the Hay−Thiebault−Hoffmann and Kahn models, antiferromagnetic contribution to the magnetic coupling constant depends on the energy gap (Δ) between the SOMOs.[36] It is well-known that the interaction or degree of mixture between the metal SOMOs and the ligand orbitals tunes this gap. So, when the metal and ligand orbitals are close in energy or when the electronic density on the bridging ligand is localized on the exchange pathway, specifically on the donor atoms, the metal−ligand interaction is stronger, leading to a larger energy gap. This is the case for the oxalate ligand but not for bipyrimidine ligand (Table 3 and Figure 8). This fact is very significant in the $x^2 - y^2$ orbital that represents the main contribution to the magnetic exchange coupling (largest energy gaps in Table 3), since its electronic density is placed mainly in the equatorial plane and is directed to the donor atoms of the bridging ligand. In

(34) (a) Price, D. J.; Powell, A. K.; Wood, P. T. *Dalton Trans.* **2003**, 2478. (b) Armentano, D.; De Munno, G.; Faus, J.; Lloret, F.; Julve, M. *Inorg. Chem.* **2001**, *40*, 655.

(35) (a) Gaspar, A. B.; Ksenofontov, V.; Martinez, V.; Munoz, M. C.; Real, J. A.; Gutlich, P. *Eur. J. Inorg. Chem.* **2004**, 4770. (b) Thetiot, F.; Triki, S.; Pala, J. S.; Galan-Mascaros, J. R.; Martinez-Agudo, J. M.; Dunbar, K. R. *Eur. J. Inorg. Chem.* **2004**, *3783*. (c) Triki, S.; Thetiot, F.; Galan-Mascaros, J. R.; Pala, J. S. *New J. Chem.* **2001**, *25*, 954.

(36) (a) Hay, P. J.; Thiebault, J. C.; Hoffmann, R. *J. Am. Chem. Soc.* **1975**, *97*, 4884. (b) Kahn, O; Briat B. *J. Chem. Soc., Faraday Trans 2* **1976**, *72*, 268. (c) Calatayud, M. L.; Castro, I.; Sletten, J.; Cano, J.; Lloret, F.; Faus, J.; Julve, M.; Seitz, G.; Mann, K. *Inorg. Chem.* **1996**, *35*, 2858. (d) Can, J.; Ruiz, E.; Alemany, P; Lloret, F.; Alvarez, S. *J. Chem. Soc., Dalton Trans.* **1999**, 1669.

summary, a larger total antiferromagnetic contribution is expected in model **ox**. This is also observed in the atomic spin densities on the metal ion, it being of lower density in model **ox** due to a larger delocalization on the ligand.

Conclusions

The work reported here demonstrates that 2-cyanopyrimidine can be hydrolyzed under hydrothermal conditions and in the presence of metal ions to afford the new bisdidentate ligand pyrimidine-2-carboxylato. The assembly of this in situ generated bisdidentate ligand with metal ions leads to the compounds $[M_2(\mu\text{-pymca})_3]OH{\cdot}H_2O$ ($M = Co^{II}$ and Fe^{II}), which constitute the first examples of 2D coordination polymers containing cationic heterochiral honeycomb networks with bisdidentate ligands. The results also show that the pymca ligand is able to efficiently transmit antiferromagnetic interaction between the metal ions, leading in the case of **1** to weak ferromagnetism (spin-canted antiferromagnet) and in the case of **2** to antiferromagnetic ordering. In addition, these cationic honeycomb magnetic networks could, in principle, be good candidates for the development of new polyfunctional magnetic materials by using template anions with interesting physical properties such as chirality, luminescence, electrical conductivity, etc. Work along this line, in hydrothermal as well as conventional solution conditions (using directly the pymca ligand), is in progress in our lab.

Acknowledgment. This work was supported by the Spanish Ministerio de Ciencia y Tecnología through project CTQ2005/0935 and Junta de Andalucía. A.R. thanks the Ministerio de Ciencia y Tecnología for a predoctoral fellowship. We also thank to Prof. A. Romerosa (University of Almería, Spain) for the X-ray crystal data collection of **1**.

Supporting Information Available: X-ray crystallographic data for the structures of **1** and **2**. This material is available free of charge via the Internet at http://pubs.acs.org.

IC061908E